transform IR (FTIR) spectroscopy (Biorad FTS6000) by the disappearance of the C–H stretching vibration peak at 2840–2970 cm^{-1}.

X-ray diffraction (XRD) patterns were taken on a RINT-2100 (Rigaku) diffractometer using Cu Kα radiation. In-plane XRD measurements were performed on an ATX-G (Rigaku) diffractometer using Cu Kα radiation.

Received: August 31, 2004
Final version: December 29, 2004
Published online: February 24, 2005

[1] C. T. Kresge, M. E. Leonowicz, W. J. Roth, J. C. Vartuli, J. S. Beck, *Nature* **1992**, *359*, 710.
[2] J. S. Beck, J. C. Vartuli, W. J. Roth, M. E. Leonowicz, C. T. Kresge, K. D. Schmitt, C. T.-W. Chu, D. H. Olson, E. W. Sheppard, S. B. McCullen, J. B. Higgins, J. L. Schlenker, *J. Am. Chem. Soc.* **1992**, *114*, 10 834.
[3] T. Yanagisawa, T. Shimizu, K. Kuroda, C. Kato, *Bull. Chem. Soc. Jpn.* **1990**, *63*, 988.
[4] S. Inagaki, Y. Fukushima, K. Kuroda, *J. Chem. Soc., Chem. Commun.* **1993**, 680.
[5] A. Stein, B. J. Melde, R. C. Schroden, *Adv. Mater.* **1997**, *12*, 1403.
[6] Q. Huo, D. Zhao, J. Feng, K. Weston, S. K. Buratto, G. D. Stucky, S. Schacht, F. Schüth, *Adv. Mater.* **1997**, *9*, 974.
[7] F. Marlow, M. D. McGehee, D. Zhao, B. F. Chmelka, G. D. Stucky, *Adv. Mater.* **1999**, *11*, 632.
[8] K. Kageyama, J. Tamazawa, T. Aida, *Science* **1999**, *285*, 2113.
[9] M. Huang, A. Choudrey, P. Yang, *Chem. Commun.* **2000**, 1063.
[10] Y. J. Han, J. M. Kim, G. D. Stucky, *Chem. Mater.* **2000**, *12*, 2068.
[11] M. Ogawa, *J. Am. Chem. Soc.* **1994**, *116*, 7941.
[12] Y. Lu, R. Ganguli, C. A. Drewien, M. T. Anderson, C. J. Brinker, W. Gong, Y. Guo, H. Soyez, B. Dunn, M. H. Huang, J. I. Zink, *Nature* **1997**, *389*, 364.
[13] H. Yang, A. Kuperman, N. Coombs, S. Mamiche-Afara, G. A. Ozin, *Nature* **1996**, *379*, 703.
[14] I. A. Aksay, M. Trau, S. Manne, I. Honma, N. Yao, L. Zhou, P. Fenter, P. M. Eisenberg, S. M. Gruner, *Science* **1996**, *273*, 892.
[15] H. Miyata, K. Kuroda, *Chem. Mater.* **1999**, *11*, 1609.
[16] H. Miyata, K. Kuroda, *Adv. Mater.* **1999**, *11*, 1448.
[17] K. Ichimura, *Chem. Rev.* **2000**, *100*, 1847.
[18] T. Seki, *Polym. J. (Tokyo, Jpn.)* **2004**, *36*, 435.
[19] Y. Kawashima, M. Nakagawa, T. Seki, K. Ichimura, *Chem. Mater.* **2002**, *14*, 2842.
[20] Y. Kawashima, M. Nakagawa, K. Ichimura, T. Seki, *J. Mater. Chem.* **2004**, *14*, 328.
[21] N. Kawatsuki, T. Kawakami, T. Yamamoto, *Adv. Mater.* **2001**, *13*, 1337.
[22] N. Kawatsuki, H. Fukumoto, O. Takeuchi, N. Furuso, T. Yamamoto, *Polymer* **2004**, *45*, 2615.
[23] A. Hozumi, Y. Yokogawa, T. Kameyama, K. Hikaru, H. Sugimura, O. Takai, M. Okido, *Adv. Mater.* **2000**, *12*, 985.
[24] N. A. Melosh, C. A. Steinbeck, B. J. Scott, R. C. Hayward, P. Davidson, G. D. Stucky, B. F. Chemelka, *J. Phys. Chem. B* **2004**, *108*, 11 909.
[25] K. K. Rangan, P. N. Trikalitis, M. G. Kanatzidis, *J. Am. Chem. Soc.* **2000**, *122*, 10 230.
[26] N. Kawatsuki, S. Sakashita, K. Takatani, T. Yamamoto, O. Sangen, *Macromol. Chem. Phys., Suppl.* **1996**, *197*, 1919.
[27] N. Nishiyama, S. Tanaka, Y. Egashira, Y. Oku, K. Ueyama, *Chem. Mater.* **2002**, *14*, 4229.

Toward the Ultimate Tribological Interface: Surface Chemistry and Nanotribology of Ultrananocrystalline Diamond**

By *Anirudha V. Sumant*, *David S. Grierson*, *Jennifer E. Gerbi*, *James Birrell*, *Uday D. Lanke*, *Orlando Auciello*, *John A. Carlisle*, and *Robert W. Carpick**

Innovations in materials synthesis and design are leading to the rapid development of micro- and nanosystems, in which structure and function are controlled down to the atomic scale.[1] In particular, micro- and nanoelectromechanical systems (MEMS/NEMS) such as optical switches, pressure sensors, and radio-frequency (rf) electromechanical resonators, hold tremendous potential. However, serious tribological issues can prevent any device that involves contacting and/or sliding interfaces from being reliable, because tribological phenomena (adhesion, friction, and wear) become critical limiting factors due to the high surface- and interface-to-volume ratios at small scales.[2] This is particularly problematic because of the lack of fundamental scientific understanding of tribology. Indeed, currently there are no commercially viable

[*] Prof. R. W. Carpick, Dr. A. V. Sumant, D. S. Grierson
Department of Engineering Physics
University of Wisconsin-Madison
Madison, WI 53706 (USA)
E-mail: carpick@engr.wisc.edu
Dr. J. E. Gerbi,[+] Dr. J. Birrell
Materials Science Division
Argonne National Laboratory
Argonne, IL 60439 (USA)
Dr. U. D. Lanke
Department of Chemistry
University of Saskatchewan
Saskatoon, SK S7N 5C9 (Canada)
Dr. O. Auciello, Dr. J. A. Carlisle
Materials Science Division and Center for Nanoscale Materials
Argonne National Laboratory
Argonne, IL 60439 (USA)
[+] Present address: Materials Science Department, University of Illinois at Urbana-Champaign, Urbana, IL 61801, USA.

[**] We gratefully acknowledge Prof. R. J. Hamers and Wensha Yang for use and assistance with the hydrogen plasma system. We gratefully acknowledge X. Xiao and J. Wang for useful discussions and input on the seeding and growth process, Prof. S. Urquhart for guidance and access to the NEXAFS system, and Dr. Suresh Varagali of Diamond Innovations for the diamond single crystal. NEXAFS was performed at the UW Synchrotron Radiation Center (supported by NSF grant DMR 0084402). The PEEM experiments were performed using the Canadian Photoelectron emission microscope which was funded by a NSERC Major Installation grant. R. W. C. acknowledges support from the National Science Foundation CAREER Program, grant #CMS-0134571, and from the Department of Energy, grant #DE-FG02-02ER46016. Work at Argonne National Labs was supported by the US Department of Energy, BES-Materials Sciences, under Contract W-13-109-ENG-38. We acknowledge support from DARPA-DSO under grant #03000Z03258. Supporting Information is available online from Wiley InterScience or from the author.

 DOI: 10.1002/adma.200401264

ADVANCED MATERIALS

MEMS/NEMS devices that involve sliding interfaces. Tribological effects are particularly challenging at the nanometer scale, where newly discovered paradigms govern interactions during contact and sliding.[3,4]

Consequently, there is a quest for MEMS/NEMS-compatible materials with excellent mechanical and tribological properties. Silicon has not yet been shown to meet the latter criteria, primarily due to its hydrophilicity, high friction, and poor wear properties. Organic coatings have been developed which alleviate the problem of adhesion,[2] but they do not yet provide reliable, long-lasting protection in sliding or impacting contacts. Diamond, in contrast, exhibits unrivalled stiffness and hardness, excellent macroscale tribological performance, highly tailorable and stable surface chemistry, excellent thermal properties, high acoustic velocity, and biocompatibility.

Surface-micromachined MEMS require the structural materials to be deposited as thin films. Diamond thin-film growth techniques and microfabrication processes are reaching a high level of maturity.[5,6] Although fabrication of diamond thin films that retain the properties of single-crystal diamond is challenging and not yet economically or technologically viable, several vigorous efforts using polycrystalline diamond in MEMS fabrication have demonstrated improvement over silicon and other conventional materials, particularly with respect to stiffness, hardness, and fracture resistance.[5,7–9] Surprisingly little attention has been devoted to either characterizing or tailoring the actual tribological interface in any contacting, sliding, diamond MEMS device. Yet, to successfully implement diamond-based MEMS/NEMS, the fundamental nanometer-scale surface properties of diamond thin films must be quantitatively determined. We stress the importance of characterizing the *underside* of a thin film, that is, the surface that becomes exposed after etching away a sacrificial underlying layer. It is this surface which would come into contact with an exposed lower layer, forming a tribological pair in a device with planar sliding.[10] Here we describe the first nanometer-scale tribological measurements of ultrananocrystalline diamond (UNCD), a diamond-based thin film that is a candidate material for MEMS/NEMS. Using tungsten carbide atomic force microscopy (AFM) tips, we show that UNCD surfaces exhibit much lower nanometer-scale adhesion and friction than ambient-exposed silicon. The surface can be further tailored via hydrogen termination to reduce adhesion to the van der Waals' limit, rendering it indistinguishable both chemically and adhesively from hydrogen-terminated single-crystal diamond as verified by surface-sensitive spectroscopy techniques. Nanometer-scale friction is also strongly reduced to the same level as single-crystal diamond. This fundamental quantitative study establishes tremendous potential for UNCD-based MEMS and NEMS.

UNCD, deposited by microwave-plasma-enhanced chemical vapor deposition (MPCVD) with a unique Ar-rich growth chemistry, is distinctive because of its nanostructure. UNCD consists of 3–5 nm sp^3-bonded diamond grains separated by narrow grain boundaries that consist of a mixture of sp^3 and sp^2 bonding.[11] Detailed studies of UNCD's microstructural, bonding, electronic, electrochemical, mechanical, and macroscopic tribological properties have been reported elsewhere.[5,12–18] Notably, the Young's modulus and hardness of UNCD are virtually equal to those of single-crystal diamond, and a friction coefficient of 0.03 has been measured in air,[19] which is also comparable to single-crystal diamond. MEMS applications under investigation include rf MEMS resonators, bio-MEMS for chemically specific sensing,[5,20] and hermetic packages for a prototype retinal prosthesis.[21] Compared with conventional polycrystalline diamond, UNCD is much stiffer, harder, tougher, and smoother, and can be grown at significantly lower temperatures. Compared with silicon, UNCD further offers the potential for extremely low friction and adhesion, without requiring hermetic packaging or elaborate molecular coatings.

UNCD films (~2 μm thick) were grown on Si substrates that were precoated with 1 μm of thermal oxide. Freestanding films were formed by etching away the substrates, and were subsequently flipped over to examine the newly exposed undersides. Some of these "bottom-side up" membranes were then treated with a hydrogen plasma. Details are provided in the Experimental section. In previous work, it was shown that this procedure preferentially etches graphitic (sp^2-bonded) carbon as well as oxygen and hydrocarbon contaminants with negligible diamond etching, leaving the surface clean and terminated with C–H bonds.[22] These "bottom-side up" membranes, along with the as-grown ("top-side up") films, were studied using scanning electron microscopy (SEM), AFM, X-ray photoelectron spectroscopy (XPS), Auger electron spectroscopy (AES), and near-edge X-ray absorption fine structure (NEXAFS) spectroscopy, to determine their surface morphology, interfacial adhesion and friction, surface chemistry, and carbon-bonding configuration.

Figures 1a,b are topographic AFM images of the as-deposited UNCD topside and as-etched underside, respectively, prior to H-plasma treatment. There are substantial differences in the morphology of these surfaces. First, there is a large difference in the root-mean-square (rms) roughness (topside: 11.1 nm; underside: 2.3 nm; measured over a 10 μm × 10 μm region). The topside exhibits the random nanometer-scale roughness characteristic of UNCD,[11] while the underside exhibits extremely smooth regions, 100–300 nm across, separated by narrow crevices. The smooth regions are collections of UNCD grains, hereafter referred to as "colonies", in which each appears to have grown outward from a single nucleation site. They are remarkably smooth, with an rms roughness of only approximately 0.9 nm. The surfaces of these colonies are slightly concave, which is due to time-varying thermal etching of the oxide substrate during growth, to be discussed separately (there is no concavity when UNCD is grown on silicon, indicating that the concavity results from etching of the silicon oxide). These colonies appear to form non-wetted shapes (flat on the bottom, rounded on the sides), meeting and merging on their sides as they grow and thus pinching off the regions now seen as crevices when viewed from the underside. The topography resembles a two-dimensional analogy of grain growth in crystals, but we emphasize here that the entities (colonies) are not single grains,

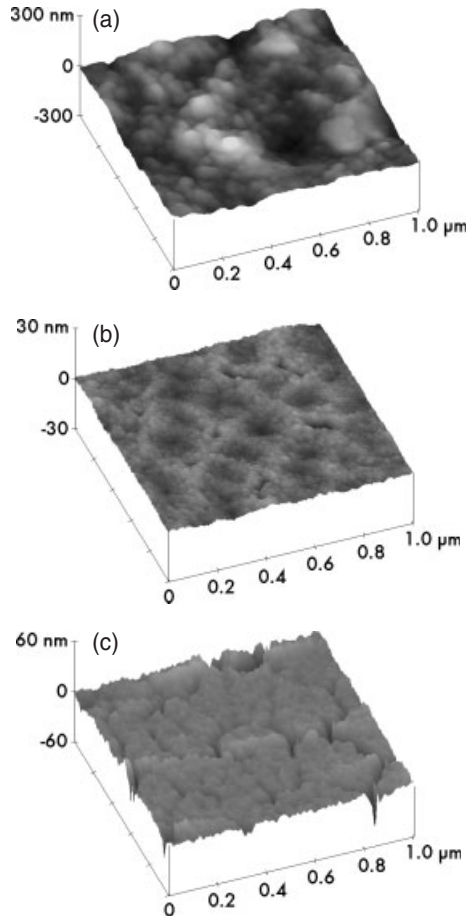

Figure 1. 1 μm × 1 μm AFM topographic images of UNCD. a) Topside, as grown. b) Underside, after etching away the substrate and before H termination. c) Underside, after H termination.

but grain clusters. Once these colonies coalesce, the remaining UNCD film grows continuously and pinhole-free, as revealed by cross-sectional TEM[23,24] and chemical-etching tests. The low intrinsic roughness of the surfaces of the colonies indicates that eliminating the crevices by achieving a higher nucleation density will produce films with an extremely low underside roughness. Recent work on enhancing the nucleation density by using a carbide-forming metallic layer appears promising and will be discussed in a future publication.

The chemistry of the topside and underside was studied using XPS. Survey spectra (not shown) taken before exposure to the hydrogen plasma revealed oxygen on both sides, with a slightly higher concentration on the underside (~12–15 at.-% vs. ~8–10 at.-% on the topside). Higher-resolution carbon-1 s spectra (Fig. 2a) confirm that some of this oxygen was chemically bonded to the carbon, as seen by a chemically shifted peak due to C–O bonds at 286.4 eV. This oxygen arises from either ambient exposure or the residual partial pressure of oxygen in the UNCD growth chamber. The oxygen concentration on the underside may also have been affected by the seeding process, the silicon oxide substrate, or the HF/HNO_3 etchant used.

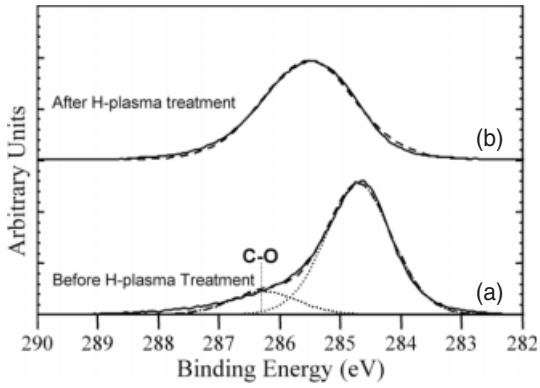

Figure 2. XPS C 1s spectra of the UNCD underside a) before and b) after H termination, for the samples shown in Figures 1b,c, respectively.

Additional surface chemical information and the carbon bonding configuration were studied using total electron yield (TEY) NEXAFS spectroscopy.[25,26] NEXAFS is particularly useful for probing the bonding configuration in nanostructured carbon materials.[27] Unlike Raman spectroscopy, it is equally sensitive to sp^3- and sp^2- bonded carbon, as well as other bonding forms. TEY NEXAFS probes the core-hole perturbed local density of unoccupied states in the first ~15 nm of the sample. Spectra obtained from single-crystal diamond and highly oriented pyrolitic graphite (HOPG) reflect the very different electronic structures in these materials (Figs. 3a,b). The HOPG (SPI Supplies, West Chester, PA) was prepared by removing the top layer with adhesive tape. The diamond single crystal (courtesy of Diamond Innovations, Worthington, OH) was a synthetically grown type IIB crystal with a (111) orientation. Carbon exhibits distinct spectral features associated with sp^3 bonding (C $1s \rightarrow \sigma^*$ transitions starting at 289.5 eV) and sp^2 bonding (C $1s \rightarrow \pi^*$ resonance at 285 eV). Like single-crystal diamond, high quality diamond thin films exhibit a sharp absorption edge at 289.5 eV. In addition, a narrow core exciton peak at 289.15 eV is observed in experiments with sufficient energy resolution.[24,27,28] For diamond, features above the C $1s \rightarrow \sigma^*$ transition at 289.5 eV represent the unoccupied states, including the second bandgap that produces a pronounced dip at ~302 eV.

Figure 3c shows the C 1s TEY NEXAFS spectrum for the UNCD topside. This sample had been treated with the H plasma, but no difference was seen between the as-grown and H-plasma-treated topside (not shown). The spectrum clearly resolves the sharp absorption edge at 289.5 eV and all expected features above it. The diamond exciton peak at 289.15 eV is known to be slightly broader than that for single-crystal diamond,[29] and appears here as a sharp corner because of our resolution limit. Separate measurements carried out using a different beam line with greater surface sensitivity and higher energy resolution (0.2–0.4 eV) clearly resolved the exciton peak, consistent with previous results.[24] The small peak due to the C $1s \rightarrow \pi^*$ resonance at 285 eV is due to a small amount of sp^2-bonded carbon. This is consistent with the observation of ~5 % sp^2 content identified in previous NEXAFS studies[29]

ADVANCED MATERIALS

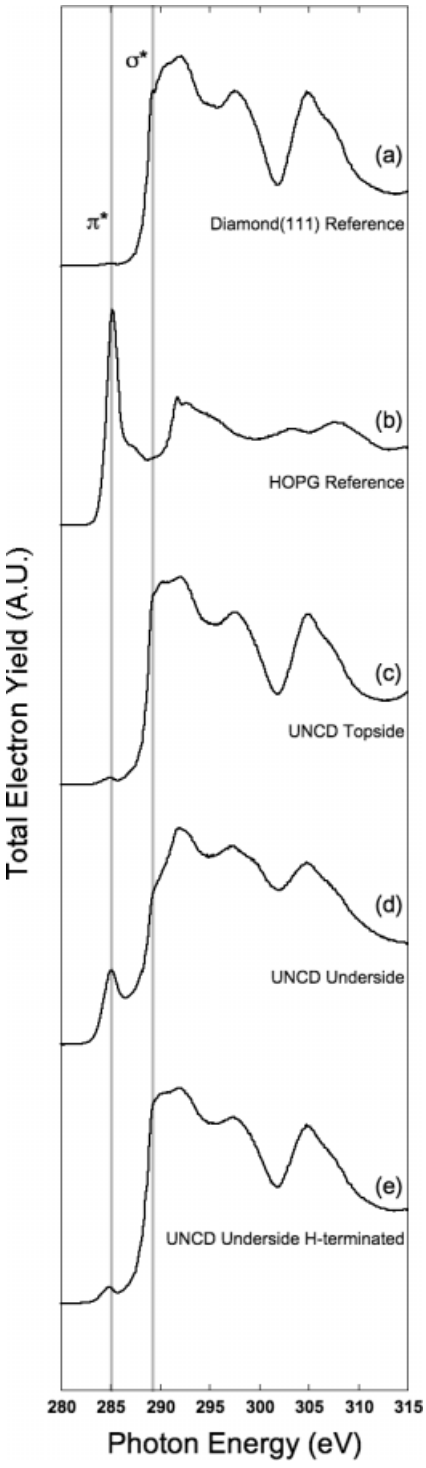

Figure 3. NEXAFS total-electron-yield spectra of a) single-crystal diamond (111) reference sample, b) HOPG reference sample, and c–e) the three UNCD samples shown in Figures 1a–c, respectively. The underside originally shows significant π-bonded carbon, which is reduced to the same level as the topside after exposure to the H plasma.

and due to the grain boundaries. This unambiguously demonstrates sp^3-bonded carbon as the dominant phase in the near-surface region of the topside.

The TEY NEXAFS spectrum from the as-etched underside of UNCD before exposure to H plasma (Fig. 3d) shows a significantly more intense C $1s \rightarrow \pi^*$ resonance peak and a less distinct diamond exciton feature, demonstrating a significant presence of graphitic or amorphous carbon. This is supported by AES studies on the same samples (not shown) and is suggested by previous cross-sectional TEM studies on a different set of UNCD films.[23,24] The manner in which this interfacial graphitic/amorphous carbon is formed is the focus of a separate study, but is possibly due to graphitization of carbon growth species in the voids between the colonies entrapped at the UNCD/substrate interface during growth.

To investigate the nanotribology of UNCD, we used AFM to study interfacial adhesion and friction between AFM tips and UNCD in ambient air, before and after H-plasma treatment. AFM can determine the true work of adhesion between two surfaces by using elastic, adhesive, single-asperity contact mechanics.[30] Two sets of measurements using partially oxidized tungsten carbide tips (MikroMasch, Portland, OR) were obtained. These measurements, using two separate tip/cantilever assemblies to test for reproducibility, were found to agree. It would be preferable to use a UNCD tip. Unfortunately, such tips are not currently available, but recent progress in our lab fabricating such tips will be discussed in a future publication. Nevertheless, tungsten carbide represents a relatively hard and stable carbide counterface. The details of these quantitative, calibrated measurements are discussed in the Experimental section and in the Supporting Information.

The work of adhesion between the tip and various samples is plotted in Figure 4a. Results for a single-crystal silicon (111) wafer with a native oxide (stored in the laboratory ambient, rinsed with acetone, methanol, and ethanol, and then stored in dry nitrogen until the measurements were performed) and for the diamond (111) single crystal are included for comparison. Si shows the highest work of adhesion. Although the clean native oxide of Si has a hydrophilic character and a high surface energy, samples which have been exposed to air, like the one used here, have a substantially reduced surface energy and even become hydrophobic, remaining so after solvent cleaning.[31] The UNCD underside before H exposure exhibited a substantially lower work of adhesion than this "passivated" form of silicon (~ 59 mJ m^{-2} vs. 115 mJ m^{-2}), comparable to that of the untreated (111) diamond surface. We also measured friction between the tungsten carbide tip and both UNCD and diamond (111). The results are plotted in Figure 4b. Friction was measured at a zero externally applied load (i.e., only adhesion held the tip onto the surface). The measured friction force for the as-etched underside is comparable to that of the untreated diamond (111) surface within the statistical error. The significant statistical errors in both the adhesion and friction data are not surprising since the actual contact area was only a few square nanometers, so small variations in sample morphology and surface chemistry could have altered individual measurements. Friction measurements on Si were avoided because sliding-induced contamination of tips rendered the measurements irreproducible.

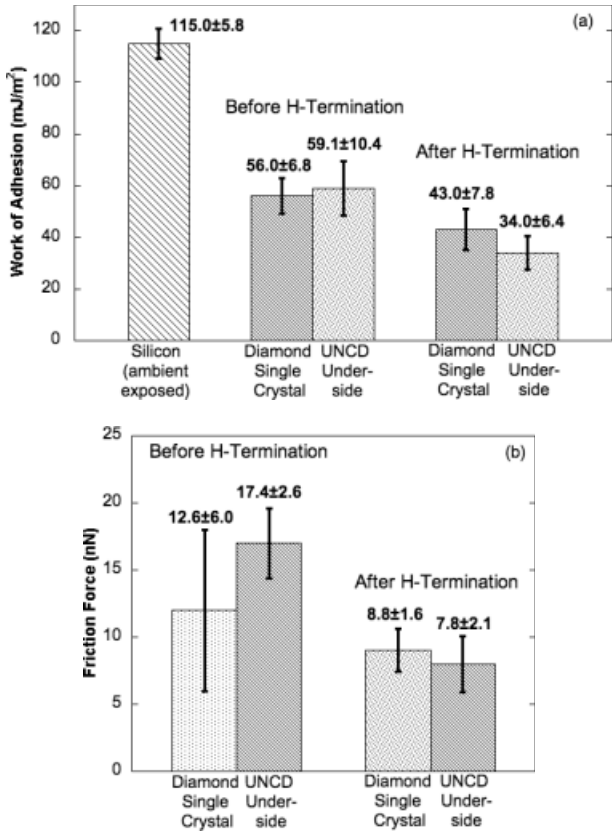

Figure 4. Graphs comparing AFM single-asperity measurements of a) the work of adhesion and b) the friction force (at zero externally applied load) of the UNCD underside and single-crystal diamond (111) before and after H termination, measured with a tungsten carbide AFM tip; measurement of the work of adhesion of solvent-cleaned single-crystal silicon is also included in (a).

The excellent properties of UNCD, including the low nanometer-scale adhesion and friction, all indicate that the underside of UNCD could significantly outperform silicon in MEMS/NEMS applications. Yet, the underside possesses somewhat more sp^2 character, more oxygen content, and less hydrogen termination than the topside. These factors may each have detrimental effects on friction, adhesion, and wear at MEMS/NEMS length scales. Molecular dynamics simulations by Harrison and co-workers[32] showed that sp^2-bonded atoms on an amorphous carbon surface lead to tribochemical reactions with a diamond tip, namely, the formation of interfacial C–C bonds, resulting in higher friction and surface damage. The loosely bonded nature of graphitic species could also lead to debris formation during sliding. In addition, oxygen increases friction with carbon-based films,[33] and thus could also contribute unfavorably. Finally, dangling bonds on diamond surfaces lead to high friction and adhesion, but these can be substantially reduced by hydrogen termination.[34–36]

An optimized diamond MEMS/NEMS interface should be composed purely of hydrogen-terminated sp^3-bonded carbon. Several methods can remove oxygenated species and graphitic carbon to achieve this chemical optimization. For this study, we applied a simple post-growth H-plasma treatment to the exposed underside, since this preferentially etches oxides and graphitically bonded carbon, and leaves diamond fully H terminated.[22,37] Figures 1c,2b,3e, respectively, show AFM, XPS, and TEY NEXAFS results for the underside taken after the H-plasma treatment. The AFM image, Figure 1c, reveals interesting morphological changes, where the crevices between the clusters of grains have become wider and deeper. Since the plasma aggressively etches graphitic carbon, this suggests that the crevices were predominantly populated by such species, as mentioned earlier. The post-treatment XPS C 1s scan, Figure 2b, shows a single peak at 285.5 eV. This represents the pure C 1s peak for the C–C bond, with no indication of a C–O bond, but shifted upward by 0.9 eV from the expected 284.6 eV due to charging on the insulating H-plasma-treated UNCD underside. A small (4 at.-%) amount of physisorbed oxygen was seen in the XPS survey scan (not shown). Similar quantities of oxygen are observed on H-terminated diamond single crystals as a result of exposure to air, and NEXAFS studies show that this can be completely removed by annealing to ~200 °C in vacuum. The TEY NEXAFS spectrum, Figure 3e, shows a large reduction in the C $1s \rightarrow \pi^*$ peak at 285.0 eV and an increase in the sharpness of the exciton feature and the absorption edge at 289.5 eV, demonstrating a reduction of graphitic carbon and an increase in local ordering of the near-surface region. These results demonstrate that the UNCD underside is significantly modified by the H-plasma treatment, leading to a nanocrystalline diamond surface with a small fraction of sp^2-bonded carbon that is entirely attributable to the grain boundaries. These data indicate that the plasma-treated underside becomes nearly chemically identical to that of the topside (both before and after the plasma treatment). An alternative process to be discussed separately, which may be more amenable to MEMS processing, is to introduce a low percentage of H_2 in situ during the initial growth stages of the UNCD film, to suppress the formation of sp^2-bonded carbon and achieve a more H-terminated underside.

The H-plasma treatment of the underside reduced the work of adhesion significantly, making it equivalent to that of the H-terminated diamond (111) crystal (Fig. 4a). The work of adhesion, 32–36 mJ m^{-2}, is very low in an absolute sense: it is comparable to values found for inert, saturated hydrocarbon interfaces,[38] which are in the range of 25–35 mJ m^{-2}. In these systems, adhesion is entirely due to van der Waals' interactions. This indicates that all other adhesion mechanisms across the interface such as chemical bond interactions, surface charge and dipole interactions, and meniscus formation, have been eliminated; we have reduced adhesion to near the van der Waals' limit. Enachescu et al.[39] measured a value for the work of adhesion of ~10 mJ m^{-2} for an oxidized tungsten carbide AFM tip on H-terminated single-crystal diamond (111) in ultrahigh vacuum. However, their cantilever was not experimentally calibrated, unlike that in the method used here, and is therefore subject to significant uncertainty. The friction force measured on UNCD is reduced by approximately a fac-

ADVANCED MATERIALS

tor of two by H termination, and is comparable to that of H-terminated diamond (111) within the measurement error. These results indicate that H-terminated UNCD is tribologically equivalent to H-terminated diamond (111) at the nanometer-scale.

In summary, we have studied the surface chemistry and nanotribology of the underside of UNCD for the first time. Careful and quantitative investigation of the surface chemistry, phase, and bonding at the tribological interface is essential, since the underside revealed by etching away the substrate was substantially different from the top as-grown surface of the same film. Compared with silicon, the underside of UNCD exhibits adhesion lower by a factor of two. It is also possible to tailor this surface by using H-plasma treatment. This minimizes adhesion to near the van der Waals' limit, and reduces friction correspondingly. Once processed in this manner, UNCD is chemically, adhesively, and tribologically indistinguishable from single-crystal diamond at the nanometer scale. A remaining issue is the extent to which the underside of MEMS/NEMS structures can be treated by a hydrogen plasma. This will depend upon how the plasma penetrates into highly confined regions. Other methods to leave the underside hydrogen-terminated, such as in-situ enrichment of the plasma with hydrogen for the initial growth stages, also appear promising.

Our methodology of characterizing the tribologically relevant underside of the film not only applies to UNCD films but is relevant to any thin-film material, including silicon, silicon carbide, and others that are being explored as alternatives for MEMS/NEMS devices. Given the critical role that surface forces play, our study provides a general methodology for characterizing and optimizing surfaces of microsystems and nanosystems.

Experimental

Substrates for UNCD growth were seeded with nanocrystalline diamond powder in an ultrasonic bath. UNCD films were grown in an IPLAS (Innovative Plasma Systems GmbH, Troisdorf, Germany) CYRRANUS I large-area reactor. The deposition parameters were Ar: 49 sccm; CH_4: 1 sccm; microwave power: 800–1200 W; chamber pressure: 150 torr (1 torr ≈ 133 Pa); substrate temperature: ~800 °C. Wafers were then sectioned into ~1 cm^2 pieces and immersed in a HF/HNO_3 (1:3) acid bath, dissolving the substrate to obtain free-standing UNCD films. When possible, these were further cleaned by rinsing in acetone, methanol, and ethanol, and retrieved using a clean Si substrate, ensuring that the newly exposed underside now faced up. To hold this membrane in place, dots of silver epoxy were applied to its sides. Some of these "bottom-side up" membranes were subsequently treated with a hydrogen plasma in an inductively coupled 13.56 MHz rf reactor for 20 min at 20 torr at 600–700 °C.

NEXAFS measurements were performed at the Synchrotron Radiation Center (University of Wisconsin-Madison). The data shown were acquired on the 10 m Toroidal Grating Monochromator (TGM) beam line. Measurements were carried out in a ultrahigh vacuum (UHV) chamber with base pressure $< 6 \times 10^{-11}$ torr. The monochromator resolution was ~0.5 eV in the region close to the carbon K edge with 100 μm slits. Spectra were taken in total electron yield (TEY) mode with the incident photon beam normal to the sample, except for the HOPG data which were taken at the "magic" angle of 54.3° to avoid orientation effects [25]. All spectra were "double normalized", first to the simultaneously recorded absorption current of a gold mesh positioned in the beam line to correct for the transmission structure of the monochromator and variations in the source light, and then to the TEY spectrum (also normalized to the mesh current) of a freshly HF-etched Si sample to correct for the signal from carbon contamination on the monochromator optics. A separate set of measurements with higher energy resolution (0.2–0.4 eV) was carried out on the HERMON beam line at the SRC on an Elmitec photoemission electron microscope (PEEM) system in TEY mode.

AFM measurements were acquired using a Digital Instruments Nanoscope IV Multimode AFM in ambient air (RH ~ 40 %) using intermittent-contact mode for imaging and contact mode for adhesion and friction measurements. Normal forces were calibrated in situ by the resonance-damping method [40]. Lateral forces were calibrated using the "wedge" method [41] for three other cantilevers from the same batch using the same AFM, and deducing their average calibration factor.

The details of the analysis procedure for the adhesion measurements are presented in the Supporting Information.

Received: August 3, 2004
Final version: November 17, 2004

[1] A. N. Cleland, *Foundations of Nanomechanics: From Solid-State Theory to Device Applications*, Springer, Berlin, Germany **2003**.
[2] R. Maboudian, W. R. Ashurst, C. Carraro, *Tribol. Lett.* **2002**, *12*, 95.
[3] R. W. Carpick, M. Salmeron, *Chem. Rev.* **1997**, *97*, 1163.
[4] *Fundamentals of Friction: Macroscopic and Microscopic Processes – Proc. of the NATO ASI on Fundamentals of Friction*, (Eds: I. L. Singer, H. M. Pollock) Kluwer, Dordrecht, The Netherlands **1992**.
[5] A. R. Krauss, O. Auciello, D. M. Gruen, A. Jayatissa, A. Sumant, J. Tucek, D. C. Mancini, N. Moldovan, A. Erdemir, D. Ersoy, M. N. Gardos, H. G. Busmann, E. M. Meyer, M. Q. Ding, *Diamond Relat. Mater.* **2001**, *10*, 1952.
[6] L. Sekaric, J. M. Parpia, H. G. Craighead, T. Feygelson, B. H. Houston, J. E. Butler, *Appl. Phys. Lett.* **2002**, *81*, 4455.
[7] T. Cagin, J. Che, M. N. Gardos, A. Fijany, W. A. Goddard, III, *Nanotechnology* **1999**, *10*, 278.
[8] J. Philip, P. Hess, T. Feygelson, J. E. Butler, S. Chattopadhyay, K. H. Chen, L. C. Chen, *J. Appl. Phys.* **2003**, *93*, 2164.
[9] O. Auciello, J. Birrell, J. A. Carlisle, J. E. Gerbi, X. Xiao, B. Peng, H. D. Espinosa, *J. Phys.: Condens. Matter* **2004**, *16*, 539.
[10] M. P. de Boer, D. L. Luck, W. R. Ashurst, R. Maboudian, *J. Microelectromech. Syst.* **2004**, *13*, 63.
[11] D. Zhou, T. G. McCauley, L. C. Qin, A. R. Krauss, D. M. Gruen, *J. Appl. Phys.* **1998**, *83*, 540.
[12] S. Bhattacharyya, O. Auciello, J. Birrell, J. A. Carlisle, L. A. Curtiss, A. N. Goyette, D. M. Gruen, A. R. Krauss, J. Schlueter, A. Sumant, P. Zapol, *Appl. Phys. Lett.* **2001**, *79*, 1441.
[13] D. M. Gruen, P. C. Redfern, D. A. Horner, P. Zapol, L. A. Curtiss, *J. Phys. Chem. B* **1999**, *103*, 5459.
[14] A. R. Krauss, O. Auciello, M. Q. Ding, D. M. Gruen, Y. Huang, V. V. Zhirnov, E. I. Givargizov, A. Breskin, R. Chechen, E. Shefer, V. Konov, S. Pimenov, A. Karabutov, A. Rakhimov, N. Suetin, *J. Appl. Phys.* **2001**, *89*, 2958.
[15] J. E. Gerbi, O. Auciello, J. Birrell, D. M. Gruen, B. W. Alphenaar, J. A. Carlisle, *Appl. Phys. Lett.* **2003**, *83*, 2001.
[16] Q. Chen, D. M. Gruen, A. R. Krauss, T. D. Corrigan, M. Witek, G. M. Swain, *J. Electrochem. Soc.* **2001**, *148*, L4.
[17] Y. Show, M. A. Witek, P. Sonthalia, G. M. Swain, *Chem. Mater.* **2003**, *15*, 879.
[18] J. E. Gerbi, J. Birrell, M. Sardela, J. A. Carlisle, *Thin Solid Films* **2005**, *473*, 41.
[19] A. Erdemir, C. Bindal, G. R. Fenske, C. Zuiker, R. Csencsits, A. R. Krauss, D. M. Gruen, *Diamond Films Technol.* **1996**, *6*, 31.

[20] W. Yang, O. Auciello, J. E. Butler, W. Cai, J. A. Carlisle, J. Gerbi, D. M. Gruen, T. Knickerbocker, T. L. Lasseter, J. N. Russell, Jr., L. M. Smith, R. J. Hamers, *Nat. Mater.* **2002**, *1*, 253.
[21] J. A. Carlisle, O. Auciello, *Electrochem. Soc. Interface* **2003**, *12*, 28.
[22] B. D. Thoms, M. S. Owens, J. E. Butler, C. Spiro, *Appl. Phys. Lett.* **1994**, *65*, 2957.
[23] S. Jiao, A. Sumant, M. A. Kirk, D. M. Gruen, A. R. Krauss, O. Auciello, *J. Appl. Phys.* **2001**, *90*, 118.
[24] D. M. Gruen, *Annu. Rev. Mater. Sci.* **1999**, *29*, 211.
[25] J. Stöhr, *NEXAFS Spectroscopy*, Springer Verlag, Berlin, Germany **1992**.
[26] H. Ade, S. G. Urquhart, in *Chemical Applications of Synchrotron Radiation, Part II*, Advanced Series in Physical Chemistry (Ed: T. K. Sham), Vol. 12b, World Scientific Publishing, Singapore **2002**.
[27] D. M. Gruen, A. R. Krauss, C. D. Zuiker, R. Csencsits, L. J. Terminello, J. A. Carlisle, I. Jimenez, D. G. J. Sutherland, D. K. Shuh, W. Tong, F. J. Himpsel, *Appl. Phys. Lett.* **1996**, *68*, 1640.
[28] A. Heiman, I. Gouzman, S. H. Christiansen, H. P. Strunk, G. Comtet, L. Hellner, G. Dujardin, R. Edrei, A. Hoffman, *J. Appl. Phys.* **2001**, *89*, 2622.
[29] J. Birrell, J. E. Gerbi, J. A. Carlisle, O. Auciello, D. M. Gruen, J. M. Gibson, *J. Appl. Phys.* **2003**, *93*, 5606.
[30] K. Johnson, J. Greenwood, *J. Colloid Interface Sci.* **1997**, *192*, 326.
[31] H. K. Christenson, *J. Phys. Chem.* **1993**, *97*, 12 034.
[32] G. T. Gao, P. T. Mikulski, G. M. Chateauneuf, J. A. Harrison, *J. Phys. Chem. B* **2003**, *107*, 11 082.
[33] J. A. Heimberg, K. J. Wahl, I. L. Singer, A. Erdemir, *Appl. Phys. Lett.* **2001**, *78*, 2449.
[34] R. van den Oetelaar, C. Flipse, *Surf. Sci.* **1997**, *384*, L828.
[35] M. N. Gardos, *Surf. Coat. Technol.* **1999**, *113*, 183.
[36] M. N. Gardos, S. A. Gabelich, *Tribol. Lett.* **1999**, *6*, 87.
[37] B. D. Thoms, J. E. Butler, *Surf. Sci.* **1995**, *328*, 291.
[38] J. N. Israelachvili, *Intermolecular and Surface Forces*, 2nd ed., Academic Press, London **1992**.
[39] M. Enachescu, R. J. A. van den Oetelaar, R. W. Carpick, D. F. Ogletree, C. F. J. Flipse, M. Salmeron, *Phys. Rev. Lett.* **1998**, *81*, 1877.
[40] J. E. Sader, J. W. M. Chon, P. Mulvaney, *Rev. Sci. Instrum.* **1999**, *70*, 3967.
[41] D. F. Ogletree, R. W. Carpick, M. Salmeron, *Rev. Sci. Instrum.* **1996**, *67*, 3298.

Boring Deep Cylindrical Nanoholes in Silicon Using Silver Nanoparticles as a Catalyst

By *Kazuya Tsujino* and *Michio Matsumura**

Silicon shows unique electrochemical properties in solutions containing hydrofluoric acid.[1–4] Cylindrical holes electrochemically formed in silicon in these solutions have recently attracted much attention due to their possible applications in photonic crystals,[5] micromachining,[6] etc. These nanoholes are generated in the <100> direction at those positions where small pits were preformed by photolithography.[7,8] Here we report that, without using an electrochemical method, cylindrical nanoholes can be generated by immersing silicon wafers loaded with Ag nanoparticles in a solution containing hydrofluoric acid and hydrogen peroxide.

We have been studying the chemical etching of silicon for making an antireflective surface structure (textured structure) in order to increase the efficiency of multi-crystalline Si solar cells.[9] In the course of this study, we found that the use of Ag nanoparticles as a catalyst is especially effective for making the textured structure. We also found that the catalysis by Ag nanoparticles results in the formation of cylindrical nanoholes in single-crystalline Si wafers when the treatment is continued for a longer time. During the process, the Ag particles gradually sink into the silicon, forming nanoholes as deep as 500 μm and with diameters of about 50 nm.

Figure 1 shows a scanning electron microscope (SEM) image of Ag particles deposited on the surface of a p-type Si(100) wafer by electroless plating (see Experimental).[10] The sizes of the particles are mostly between 30 nm and 100 nm. There was no significant difference between the p-type and n-type wafers in densities and size distributions of the deposited Ag particles. In addition, the (100) and (111) orientations did not affect the Ag deposition. Other metal particles were also deposited on Si wafers from solutions containing metal ions, such as Pt, Pd, and Cu.

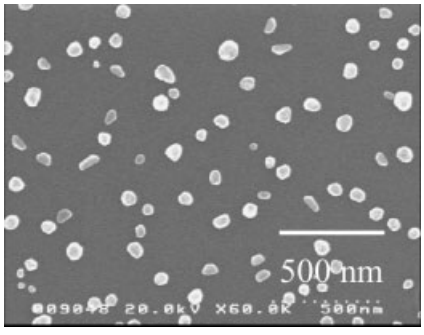

Figure 1. Scanning electron microscopy (SEM) image of Ag particles deposited on a p-type Si(100) wafer by electroless plating.

After the deposition of these metal particles, the Si wafers were etched in a mixed solution of 10 % HF and 30 % H_2O_2 (10:1 v/v) for 30 min in the dark at room temperature. The etched surface of the Si wafers was covered with a microporous Si layer. The microporous Si layer became as thick as 3 μm when Pt particles were used as the catalyst, and showed orange photoluminescence under UV irradiation at 265 nm. Since Pt has a strong catalytic activity in the reduction of hydrogen peroxide,[11] it is assumed that valence-band electrons in Si are drawn through the Si/metal interface as hydrogen peroxide is reduced. As a result, positively charged holes are generated in the Si, leading to the formation of a microporous

[*] Prof. M. Matsumura, K. Tsujino
Research Center for Solar Energy Chemistry
Osaka University
1–3 Machikaneyama, Toyonaka, Osaka 560-8531 (Japan)
E-mail: matsu@chem.es.osaka-u.ac.jp

 DOI: 10.1002/adma.200401681